Precision monitoring of vine water stress using UAVs and open-source processing chains

V. Burchard-Levine[1*], H. Nieto[1], G.A. Mesías-Ruiz[1], J. Dorado[1], A.I. de Castro[2], and J.M. Peña[1]
[1]*Tec4Agro, Institute of Agricultural Sciences (ICA), Spanish National Research Council (CSIC), Madrid, Spain*
[2]*Environment and Agronomy Department, National Agricultural and Food Research and Technology Institute-INIA, Spanish National Research Council (CSIC), Madrid, Spain*
*vburchard@ica.csic.es

Abstract

This work aimed to evaluate the potential of visible-near-infrared (VNIR) and thermal infrared (TIR) imagery, acquired from an unmanned aerial vehicle (UAV), to detect vine water status. Three irrigation treatments were designed to impose weekly evapotranspiration (ET) to $K_C = 0.2$, $K_C = 0.4$ and $K_C = 0.8$ of reference ET. *In-situ* leaf area index (LAI) and midday leaf (Ψ_{Leaf}) and stem water potential were collected during seven UAV overpasses. TIR-based temperature correlated highly with the water status variability observed between treatments (Ψ_{Leaf}: $r = -0.68$). However, VNIR indices were less correlated with Ψ_{Leaf} ($r < 0.4$), revealing the importance of TIR imaging to capture the vine physiological response to water stress, with foliage differences being less apparent between treatments.

Keywords: remote sensing, irrigation, vineyards, thermal infrared, multispectral

Introduction

More than 7 Mha of the Earth's surface is devoted to grapevine production according to the *Organisation International de la Vigne et du Vin* (OIV, 2022), occupying a particular historical, cultural and economic importance in the Mediterranean region (Limier et al., 2018). While vineyards have traditionally been cultivated through rainfed conditions, irrigation practices are becoming increasingly widespread in the Mediterranean basin, particularly due to the increase of extreme heat and drought events stemming from climate change (Rienth & Scholasch, 2019; Romero et al., 2022).

The precise quantification of water availability and vine water status is therefore essential to provide guidelines on agronomic management solutions to optimize grape production in light of these changing conditions. In recent years, large advances have been made in the use of unmanned aerial vehicles (UAV) to support the precise monitoring of agronomic activities (e.g., de Castro et al., 2021). Particularly, the use of UAVs in conjunction with visible-near-infrared (VNIR) and thermal infrared (TIR) sensors have shown great promise to monitor vine water stress (Bellvert et al., 2014; Kustas et al., 2022). VNIR sensing has been well established in the retrieval of vegetation traits, while TIR imaging can capture vegetation physiological response through its relationship with transpiration and, thus, crop water use. Although, there is still a greater need to fully evaluate the radiometric accuracy of UAV sensors (Fawcett et al., 2020) and

how this may impact the capabilities of these systems to provide adequate agronomic management solutions. A particular bottleneck in this regard is the 'black box' nature of most conventional drone processing software (i.e. Pix4D, Agisoft Metashape). This not only limits the ability to improve UAV-based remote sensing applications for crop monitoring but is also an economic and scientific barrier to many potential researchers and early-adopters.

The main objective of this study was to evaluate the capabilities of a UAV-based payload using VNIR and TIR sensors to track water stress over grapevines treated with different irrigation regimes, through the use of fully open-source processing chains (i.e. OpenDroneMap). Remote sensing-based vegetation indicators were benchmarked against in-situ biophysical measurements collected during UAV overpasses.

Materials and Methods

The case study was implemented in a 0.5 ha vineyard (*Petit Verdot*) located at the 'El Socorro' experimental farm (Belmonte de Tajo, Madrid, Spain; altitude 755 m.a.s.l.) in central Spain. The area is characterized by a typical semi-arid continental Mediterranean climate with mean annual air temperatures of about 14°C and average annual rainfall of 420 mm (Guerra et al., 2022). In 2021, a drip irrigation system was installed to allow variable and precise irrigation application to study the effect of water stress on grapevines. The experimental design was established following a randomized block design with three replications for three different treatments (Fig. 1). The three different irrigation treatments consisted on maintaining different crop coefficient (K_C) compared to the reference ET (ET_0) as calculated by the FAO Penman-Monteith method (Allen et al., 1998) using daily meteorological data from a nearby tower. The irrigation period in 2022 began in early June and ended at the end of September, where irrigation inputs were adjusted weekly over the three treatments in order to maintain a Kc of 0.2 ($0.2K_C$, under-irrigated), 0.4 ($0.4K_C$, control) and 0.8 ($0.8K_C$, over-irrigated).

Figure 1. Aerial view of the El Socorro farm (a), scheme with the 3 different irrigation treatments distributed in 3 blocks and 36 vine rows (b), and construction of the drip irrigation system (c, d).

Seven field campaigns (Jun-21, Jul-05, Jul-19, Aug-02, Aug-16, Aug-30, Sept-19) were carried out during the 2022 vine phenological period to acquire UAV imagery and in-situ vine biophysical measurements. Three permanent sampling points (i.e. vines) spaced evenly at each repetition (3) of each treatment (3) resulted in a total of 27 field measurement points in each campaign. Midday leaf (Ψ_{Leaf}) and stem (Ψ_{Stem}) water potential were measured at each sampling point using Scholander pressure chamber. In

addition, leaf area index (LAI) measurements using the Licor LAI-2200C (LICOR Bioscience USA, 2011) were acquired following the protocol established for vineyards suggested by White et al. (2019). A *DJI Matrice 300* UAV (https://www.dji.com/matrice-300) was used to acquire visible-near-infrared (VNIR) and thermal infrared (TIR) imagery using a multispectral Parrot Sequoia+ (https://www.parrot.com/us/support/documentation/sequoia) along with a DJI Zenmuse H20T (https://www.dji.com/zenmuse-h20-series), respectively. Both sensors jointly acquired images at 40-50 m above surface with a 70% overlap, resulting in a native pixel resolution of between 3-5cm.

Ortho-mosaics were processed using OpenDroneMap (https://www.open-dronemap.org/), an open-source drone processing software (source code is available at https://github.com/OpenDroneMap/ODM). VNIR data from Sequoia were radiometrically calibrated using camera correction and a downwelling irradiance sensor (see https://docs.opendronemap.org/arguments/radiometric-calibration/). Three vegetation indices (VIs) were selected that exploited the different spectral bands available on the Sequoia sensor. The normalized difference vegetation index (NDVI, eq. 1, Rouse et al., 1974) is the most widely used VI and has been been shown to correlate with vegetation density (e.g. Gitelson, 2004). The optimized soil-adjusted vegetation index (OSAVI, eq. 2, Rondeaux et al., 1996) was proposed to limit the effect of soil reflectance on the NDVI signal, especially for conditions of low vegetation cover. The red-edge NDVI (reNDVI, eq. 3, Gitelson and Merzlyak 1994), was also selected since red-edge bands tend to be less affected by the canopy structure (e.g. Dong et al., 2019).

$$NDVI = \frac{pNIR - pRED}{pNI + pRED} \quad (1)$$

$$OSAVI = \frac{pNIR - pRED}{pNIR + pRED + 0.16} \quad (2)$$

$$reNDVI = \frac{pNIR - pRedEdge}{pNIR + pRedEdge} \quad (3)$$

where pNIR, pRedEdge and pRED are the reflectance factors of band 4 (~790 nm), band 3 (~735 nm) and band 2 (~660 nm) of the Sequoia sensor, respectively. Raw TIR H20T image tiles (i.e. in R-JPEG format) were converted to a single band radiometric temperatures using the open-source DJI Thermal SDK software (https://www.dji.com/downloads/softwares/dji-thermal-sdk). These individual temperature image tiles were then mosaicked together with OpenDroneMap. The resulting ortho-mosaic represented the at-sensor radiometric brightness temperature (BT) as emissivity was maintained at 1 and no atmospheric corrections were applied. Grapevine pixels were extracted by first classifying the image into three main classes: vegetation, soil and shadows using a random forest (RF) image classifier method, implemented using the scikit-learn (https://scikit-learn.org/stable/index.html) Python package. The RF model was trained using all four of Sequoia's multispectral bands over 30 points manually selected over each class (total of 90 points). Vegetation pixels were then extracted by further discarding pixels with NDVI values less than 0.2 to limit crown edge pixels that may be affected by soil/shadow interference. Furthermore, a digital surface model from a 3D point clouds derived from concurrent high-resolution RGB camera (DJI P1, https://www.dji.com/zenmuse-p1) was used to extract only vegetation pixels with canopy height greater than 0.75 m to filter out vegetation pixels associated to weeds.

Using this procedure, vine pixels were selected for each block (three treatments with three repetitions) for all dates assessed (total N = 63) to perform the statistical analyses. These analyses examined whether significant differences within vine water status indicators were apparent between irrigation treatments on both UAV-based radiometric indicators and in-situ measurements. A repeated two-way analyses of variance (ANOVA) was performed using treatments and time (i.e. sampling dates) as independent variables. Along with this, post-hoc analysis with pairwise t-tests examined how the different treatments and dates differed and interacted with each other. In-situ measurements of Ψ_{Leaf}, Ψ_{Stem} and LAI, along with the three VIs and BT, were used as dependent variables to examine how the different UAV-based indicators captured the different treatment effects. Furthermore, linear regression models were developed between in-situ measurements and VIs to assess their relation and the predictive power of the UAV system to estimate vegetation biophysical indicators.

Results and Discussion

Mean values of Ψ_{Leaf}, Ψ_{Stem} and LAI for each treatment and sampling date, along with boxplots grouped by treatment, are shown in Fig. 2. The repeated two-way ANOVA showed significant differences for Ψ_{Leaf} between treatments (F-Score = 106.9; $p = 0.008$) and sampling dates (F-Score = 60.3; $p = 0.002$). However, the interactions between both terms were not significant ($p = 0.2$). The post-hoc analysis also revealed significant pairwise differences between the three treatments ($0.2K_C$ vs $0.4K_C$: $p = 0.02$; $0.2K_C$ vs $0.8K_C$: $p = 0.003$; $0.4K_C$ vs $0.8K_C$: $p = 0.02$;). Significant treatment effects were also found for Ψ_{Stem} (F-Score = 34.1; $p = 0.015$) along with a significant sampling date effect (F-Score = 177.4; $p = 0.004$). As Fig. 2e shows, there were clear differences between treatments on all dates except on September 16th, where Ψ_{Stem} values between treatments converged together. Recent irrigation and rainfall inputs prior to the field campaign on September 16th likely reduced the overall grapevine water stress (i.e. Fig. 2d) and contributed to the convergence of both Ψ_{Stem} and Ψ_{Leaf} on this date. Post-hoc pairwise t-tests showed that the mean values were most significantly different between 0.2 and 0.8 K_C treatments ($p = 0.01$), followed by 0.4 and 0.8 K_C ($p = 0.04$) and then 0.2 and 0.4 K_C ($p = 0.09$). It should be noted that in-situ Ψ_{Stem} sampling began on July 19th campaign so there are fewer sample points compared to Ψ_{Stem} and LAI.

For LAI, borderline non-significant effects were found for both treatments (F-Score = 6.45; $p = 0.09$) and dates (F-Score = 7.29; $p = 0.05$), while the interactions of both were not significant (F-Score: 2.50; $p = 0.25$). LAI values between the $0.2K_C$ and $0.4K_C$ treatments were very similar throughout the period assessed (Fig. 2f) and their differences were highly insignificant ($p = 0.89$). The $0.8K_C$ treatment showed larger differences compared to both $0.2K_C$ ($p = 0.19$) and $0.4K_C$ ($p = 0.21$), visually apparent during the peak summer period (starting from the July 19th campaign as seen in Fig. 2f). However, these results suggest that changes to vine foliage density were not as sensitive to water stress, with non-significant treatment effects on LAI. Only the over-irrigated (i.e. $0.8K_C$) treatment showed important differences during the peak and late summer period (Fig. 2f), but overall differences were not. Mean LAI values were 1.81 and 1.85 m^2/m^2 for $0.2K_C$ and $0.4K_C$, respectively which were much lower to the mean 2.49 m^2/m^2 observed in $0.8K_C$. By contrast, both Ψ_{Stem} and Ψ_{Leaf} showed more consistent and significant

differences between treatments. These in-situ measurements confirm an important physiological response from the grapevines to the induced water stress, which did not translate as significantly to alterations in vine foliage density.

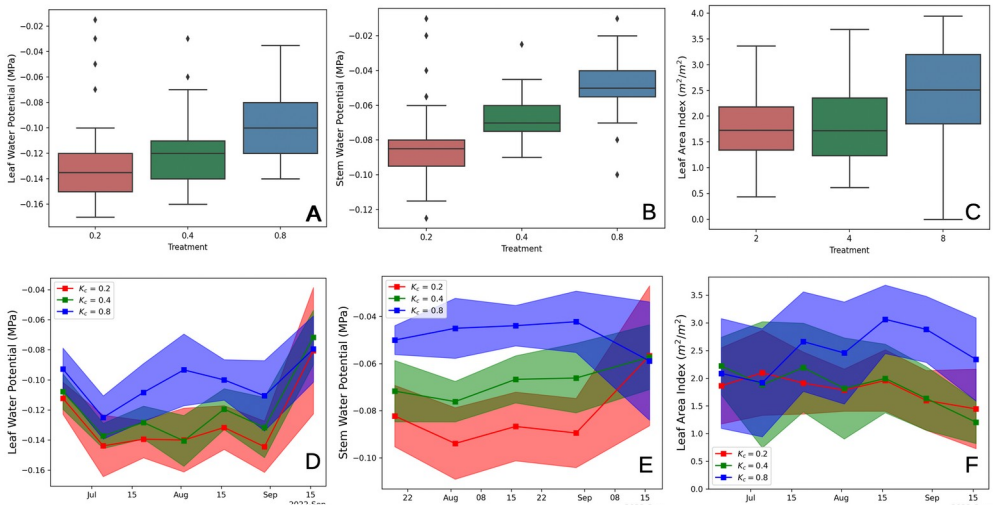

Figure 2. Boxplots grouped by treatment (0.2K_C - red, 0.4K_C -green and 0.8K_C-blue) for in-situ measurements of (a) leaf water potential (Ψ_{Leaf}), (b) stem water potential (Ψ_{Stem}) and (c) leaf area index (LAI). Mean and standard deviation of (d) Ψ_{Leaf}, (e) Ψ_{Stem} and (f) LAI over the UAV overpass dates.

Radiometric VIs from the UAV payload showed similar responses to the treatments as compared to the in-situ measurements (Fig. 3). To make comparisons more robust, BT was normalized on each overpass (nBT), using minimum and maximum vine pixel values, to limit differences in BT between dates due to meteorological conditions. ANOVA revealed significant differences due to irrigation treatments for all indices (p <0.001). NIR-based VIs showed a similar to response to LAI observations, where mean values of NDVI and OSAVI were very similar between treatments 0.2K_C and 0.4K_C (i.e. mean NDVI values were 0.42 and 0.43, respectively) while the 0.8K_c treatment had consistently higher values (i.e. mean NDVI = 0.49).

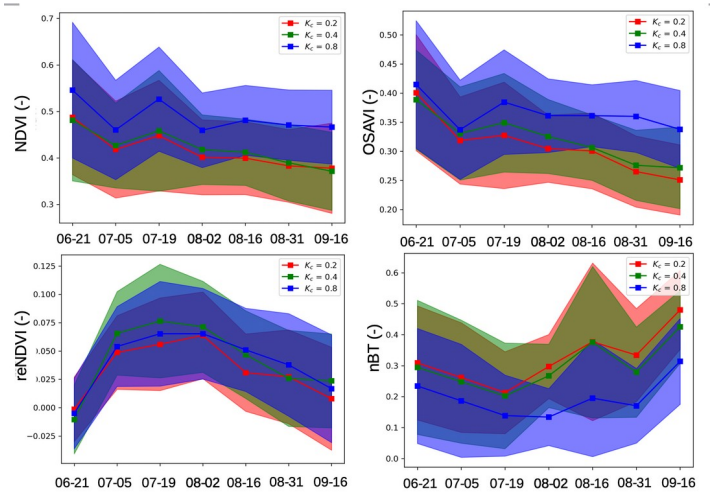

Figure 3. Time-series, grouped by treatment (0.2K_C - red, 0.4K_C -green and 0.8K_C-blue), for derived VNIR-based vegetation indices and normalized brightness temperature (nBT).

By contrast, reNDVI showed a somewhat different response to the treatments and had different temporal pattern compared to NDVI and OSAVI (Fig. 3). reNDVI values experienced larger decreases in $0.2K_C$ (mean reNDVI = 0.04) but smaller differences were observed between $0.4K_C$ (mean reNDVI = 0.047) and $0.8K_C$ (mean reNDVI = 0.046). The sequoia red-edge band was reported by Fawcett et al. (2020) to have significant offsets compared to field spectroscopy. As such, further radiometric evaluation is needed to better understand the potential of the red-edge band for grapevine precision monitoring. Differences between $0.2K_C$ and $0.4K_C$ were slightly more apparent with BT, with the mean nBT increasing to 0.33 compared to 0.29 in $0.4K_C$. Large differences were also observed between the mean nBT in $0.4K_C$ and $0.8K_C$ (mean nBT decreased to 0.19 in $0.8K_C$). The treatment differences for nBT were also relatively consistently maintained throughout the phenological period, while being more pronounced from august onwards (Fig. 3).

Fig 4. shows significant and negative correlations between BT with both Ψ_{Leaf} ($r = -0.68$; $p < 0.001$) and Ψ_{Stem} ($r = -0.5$; $p < 0.001$). It is somewhat surprising that Ψ_{Stem} were less correlated to BT as compared to Ψ_{Leaf} (although both were significant) since in-situ Ψ_{Stem} were more sensitive to irrigation treatments (Fig. 2). However, there were also fewer Ψ_{Stem} measurements since field sampling for this variable only began from the July 19th campaign onwards, therefore statistical results may be affected by a smaller sample size. By contrast, VNIR-based indices were much less correlated with Ψ_{Leaf} ($r < 0.4$) and Ψ_{Stem} ($r < 0.35$). VNIR indices generally correlated well with LAI (e.g., OSAVI: $r = 0.51$, $p < 0.001$) while BT observed no relationship with LAI ($r = -0.04$, $p = 0.74$).

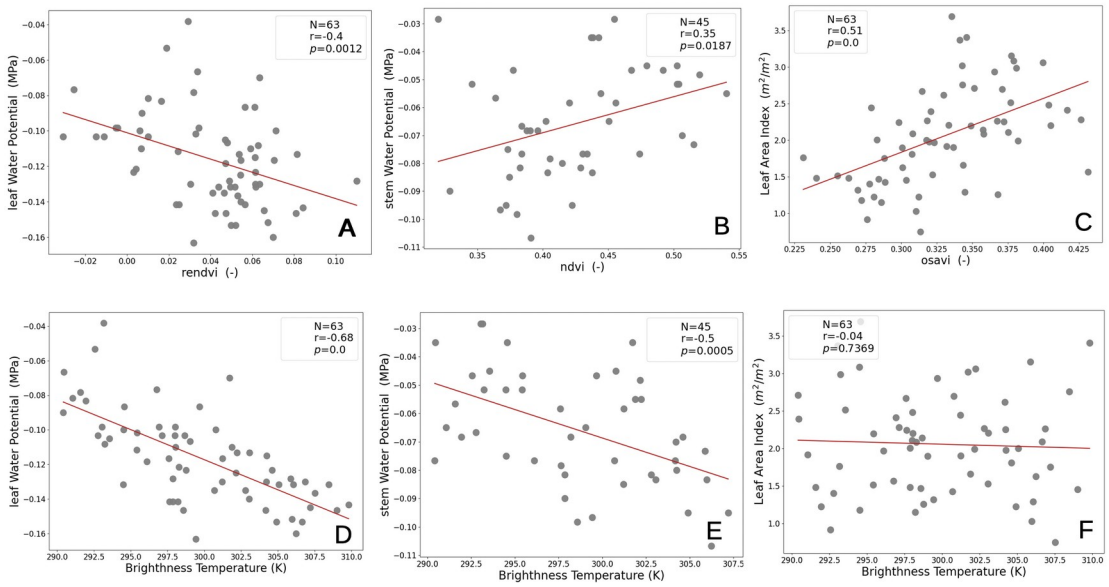

Figure 4: Figure 4. Linear regression models developed between in-situ measurements (leaf and stem water potential and leaf area index) and (a-c) VNIR indices and (d-f) brightness temperature. Best performing VNIR index is shown in figure.

This demonstrated the importance of TIR imaging to monitor vine water status, as also discussed in Bellvert et al. (2014). VNIR data were less capable to explain the variability of *in-situ* water potential measurements. Since TIR information is directly related to stomatal closure, it is more suited to capture the crop water status and its

physiological response as compared to VNIR imaging, which is more suited to monitor crop traits related to foliage structure or density. Indeed, changes to crop foliage may not react as quickly to water stress as compared to crop transpiration, as shown from the in-situ data taken throughout the main vine foliage period. By contrast, VNIR indices were found to significantly correlate with LAI, which plays an important role in the canopy radiation interception and, thus, on the partitioning of evapotranspiration (ET) between soil evaporation and plant transpiration. In fact, accurate LAI has been shown to be a critical factor in remote sensing-based ET modeling schemes, especially for ET partitioning (Kustas et al., 2019). Therefore, results from this study suggest the combined use of TIR and VNIR imaging within a UAV payload has good potential to estimate vine transpiration and give quantitative irrigation recommendations.

Conclusion

The grapevines demonstrated a notable physiological response to the different irrigation treatments through significant differences within *in-situ* water potential observations, but structural changes in foliage were not as sensitive to water stress as suggested by the field LAI measurements. Notably, changes in foliage density were mostly apparent for the over-irrigated treatment (i.e. 0.8Kc), however a non-significant treatment effect was found for LAI measurements. UAV-based TIR acquisitions were better able to track the different water status levels, having significant correlations with field acquisitions of water potential, in particular with Ψ_{Leaf}. In contrast, VNIR-based VIs were found to not relate well with the crop physiological response to water stress but seem to have potential predictive power to estimate crop foliage density (i.e. LAI). These results suggest that this relatively low cost and open source UAV processing chain has large potential to quantify vine water stress through, for example, the combined use of VNIR and TIR imaging for precise transpiration retrievals.

Acknowledgements

This research was supported by the DATI project (PCI2021-121932) from the Spanish Ministry of Science and Innovation (AEI/10.13039/501100011033) and the PRIMA EU program.

References

Allen, R. G., Pereira, L.S., Raes, D., and Smith, M. (1998). Crop Evapotranspiration-Guidelines for Computing Crop Water Requirements-FAO Irrigation and Drainage Paper 56, *FAO, Rome*, 300.9, D05109

Bellvert, J., Zarco-Tejada, P. J. , Girona, J. and Fereres, E. (2014). Mapping Crop Water Stress Index in a "Pinot-Noir" Vineyard: Comparing Ground Measurements with Thermal Remote Sensing Imagery from an Unmanned Aerial Vehicle, Precision Agriculture, 15.4 (2014), 361–76

de Castro, A. I., Shi, Y., Maja, J.M., and Peña, J.M. (2021). UAVs for Vegetation Monitoring: Overview and Recent Scientific Contributions', Remote Sensing, 13.11, 2139

Dong, T. Liu, J., Shang, J., Qian, B., Ma, B., Kovacs, J.M. et al. (2019). Assessment of Red-Edge Vegetation Indices for Crop Leaf Area Index Estimation, Remote Sensing of Environment, 222, 133–43.

Fawcett, D., Panigada, C., Tagliabue, G., Boschetti, M., Celesti, M., Evdokimov, A. et al. (2020). Multi-Scale Evaluation of Drone-Based Multispectral Surface Reflectance and Vegetation Indices in Operational Conditions, Remote Sensing, 12.3, 514.

Gitelson, A. A. (2004). Wide Dynamic Range Vegetation Index for Remote Quantification of Biophysical Characteristics of Vegetation, *J*ournal of Plant Physiology, 161.2, 165–73

Gitelson, A., and Merzlyak, M. N. (1994). Spectral reflectance changes associated with autumn senescence of Aesculus hippocastanum L. and Acer platanoides L. leaves. Spectral features and relation to chlorophyll estimation. Journal of Plant Physiology, *143*(3), 286–292.

Guerra, J. G., Cabello, F., Fernández-Quintanilla, C., Peña, J.M. and Dorado, J. (2022). Use of Under-Vine Living Mulches to Control Noxious Weeds in Irrigated Mediterranean Vineyards, Plants, 11.15, 1921

Kustas, W. P., McElrone, A.J., Agam, N. and Knipper, K. (2022). From Vine to Vineyard: The GRAPEX Multi-Scale Remote Sensing Experiment for Improving Vineyard Irrigation Management, Irrigation Science, 40.4, 435–44

Kustas, W.P., Alfieri, J.G., Nieto, H., Wilson, T.G. , Gao, F., and Anderson, M.C. (2019). Utility of the Two-Source Energy Balance (TSEB) Model in Vine and Interrow Flux Partitioning over the Growing Season, Irrigation Science, 37, 375–88

LICOR Bioscience USA (2011). LAI-2200 Plant Canopy Analyzer. Instruction Manual.

Limier, B., Ivorra, S., Bouby, L., Figueiral, I., Chabal, L., Cabanis, M. et al. (2018). Documenting the History of the Grapevine and Viticulture: A Quantitative Eco-Anatomical Perspective Applied to Modern and Archaeological Charcoal, *Journal of Archaeological Science*, 100, 45–61

OIV (2022). State of the World Vine and Wine Sector 2021. Available at: https://www.oiv.int/sites/default/files/documents/eng-state-of-the-world-vine-and-wine-sector-april-2022-v6_0.pdf (accessed February 8th 2023).

Rienth, M. and Scholasch, T. (2019). State-of-the-Art of Tools and Methods to Assess Vine Water Status, *Oeno One*, 53.4.

Romero, P., Navarro, J.M. and Ordaz, P.B. (2022). Towards a Sustainable Viticulture: The Combination of Deficit Irrigation Strategies and Agroecological Practices in Mediterranean Vineyards. A Review and Update, Agricultural Water Management, 259, 107216

Rondeaux, G., Steven, M. and Baret, F. (1996). (1996). Optimization of Soil-Adjusted Vegetation Indices, Remote Sensing of Environment, 55.2 (1996), 95–107

Rouse, J. W., Rüdiger H. Haas, John A. Schell, and Donald W. Deering, 'Monitoring Vegetation Systems in the Great Plains with ERTS', *NASA Special Publication*, 351.1974 (1974), 309

White, W. A., Alsina, M.M., Nieto, H., McKee, L.G., Gao, F. and Kustas, W.P. (2019). Determining a Robust Indirect Measurement of Leaf Area Index in California Vineyards for Validating Remote Sensing-Based Retrievals, Irrigation Science, 37.3 (2019), 269–80.